Entropy, fidelity, and double orthogonality for resonance states in two-electron quantum dots

Federico M. Pont,[1,*] Omar Osenda,[1,†] Julio H. Toloza,[2,‡] and Pablo Serra[1,§]

[1]*Facultad de Matemática, Astronomía y Física, Universidad Nacional de Córdoba, and IFEG-CONICET, Ciudad Universitaria, X5016LAE Córdoba, Argentina*

[2]*IMIT–CONICET, Universidad Nacional del Nordeste, Avenida Libertad 5400, W3404AAS Corrientes, Argentina*

Resonance states of a two-electron quantum dots are studied using a variational expansion with both real basis-set functions and complex scaling methods. The two-electron entanglement (linear entropy) is calculated as a function of the electron repulsion at both sides of the critical value, where the ground (bound) state becomes a resonance (unbound) state. The linear entropy and fidelity and double orthogonality functions are compared as methods for the determination of the real part of the energy of a resonance. The complex linear entropy of a resonance state is introduced using complex scaling formalism.

PACS number(s): 31.15.ac, 03.67.Mn, 73.22.−f

I. INTRODUCTION

In the past few years the application of quantum information concepts to some long-standing problems has led to a deeper understanding of those problems [1] and, as a consequence, to the formulation of new methods to solve (or calculate) them. For example, the simulability of many-body problems is determined by the amount of entanglement shared between the spins of the system [2].

There is a number of quantities that can be calculated in order to analyze the information carried by a given state, including the entanglement of formation [3], the fidelity [4], and several kinds of entropies, entanglement witnesses, and so on. Of course, it depends on the problem which quantity is more adequate, or accessible, to be calculated.

In the case of atomic or few-body systems with continuous degrees of freedom a rather natural quantity is the von Neumann entropy, which has been used to study a number of problems such as the helium-like atom [5,6], generation of entanglement via scattering [7], the dynamical entanglement of small molecules [8], and entanglement in Hooke's atom [9].

In quantum dots, most quantum information studies focus on the amount of entanglement carried by its eigenstates [10,11] or on the controllability of the system [12]. Both approaches are driven by the possible use of a quantum dot as the physical realization of a qubit [13]. The controllability of the system is usually investigated (or performed) between the states with the lowest lying eigenenergies [14].

Besides the possible use of quantum dots as quantum information devices there are proposals to use them as photodetectors. The proposal is based on the use of resonance states because of its properties—in particular its large scattering section compared with the scattering sections of bound states [15].

The resonance states are slowly decaying scattering states characterized by a large but finite lifetime. Resonances are also signaled by sharp, Lorentzian-type peaks in the scattering matrix. In many cases of interest where complex scaling

(analytic dilatation) techniques can be applied, resonances energies show up as isolated complex eigenvalues of the rotated Hamiltonian [16]. Under this transformation, the bound states remain exactly preserved and the resonance states are exposed as $\mathcal{L}^2$ functions of the rotated Hamiltonian. Resonance states can be observed in two-electron quantum dots [15,17] and two-electron atoms [18].

Recently, a publication by Ferrón, Osenda, and Serra [19] discussed the behavior of the von Neumann entropy associated with $\mathcal{L}^2$ approximations of resonance states of two-electron quantum dots. In particular, that work focused on the resonance state that arises when the ground state loses its stability; that is, the quantum dot does not have two-electron bound states any more. Varying the parameters of the quantum dot allows the energy to cross the ionization threshold that separates the region where the two-electron ground state is stable from the region where the quantum dot loses one electron.

In Ref. [19] it was found that the von Neumann entropy provides a way to obtain the real part of the energy of the resonance; in other words, the von Neumann entropy provides a stabilization method. The numerical approximation used in [19] gives only a reduced number of energy levels (in a region where the spectrum is continuous); their method provided the real part of the energy of the resonance only for a discrete set of parameters and this set could not be chosen *a priori*. Notwithstanding this, Ferrón *et al.* conjectured that there is a well-defined function $S(E_r)$, the von Neumann entropy of the resonance state, which has a well-defined value for every value of the real part of the energy of the resonance, E_r.

In this work, we will show that if λ is the external parameter that drives the quantum dot through the ionization threshold, then the entropy $S[E_r(\lambda)]$ is a smooth function of λ. Also, it is shown that the resonance-state entropy calculated by Ferrón *et al.* is correct near the ionization threshold.

We have studied other quantities, besides the entropy, that are good witnesses of resonance presence. One of them is the fidelity, which has been widely used [20–22] in the detection of nonanalytical behavior in the spectrum of quantum systems. The analysis of the fidelity provides a method to obtain the real part of the resonance energy from variational eigenstates. We introduce the double-orthogonality function (DO) that measures changes in quantum states and detects the resonance region. The DO compares the extended continuum states and

*pont@famaf.unc.edu.ar

†osenda@famaf.unc.edu.ar

‡jtoloza@exa.unne.edu.ar

§serra@famaf.unc.edu.ar

the state near the resonance, also providing the real part of the resonance energy.

The article is organized as follows. In Sec. II, we present the model and briefly explain the technical details to obtain approximate eigenvalues, eigenfunctions, and the density of states for the problem. In Sec. III, the fidelity is used to obtain the real part of the resonance energy and the DO is introduced as an alternative method. In Sec. IV, the linear entropy and the expectation value of the Coulomb repulsion are studied using complex scaling methods. Finally, in Sec. V, we discuss our results and present our conclusions.

II. THE MODEL AND BASIC RESULTS

There are many models of quantum dots with different symmetries and interactions. In this work, we consider a model with spherical symmetry, with two electrons interacting via the Coulomb repulsion. The main results should not be affected by the particular potential choice as it is already known that the near-threshold behavior and other critical quantities (such as the critical exponents of the energy and other observables) are mostly determined by the range of the involved potentials [23]. Therefore, to model the dot potential we use a short-range potential suitable to apply the complex scaling method. After these considerations, we propose the following Hamiltonian H for the system:

$$H = -\frac{\hbar^2}{2m}\nabla_{\mathbf{r}_1}^2 - \frac{\hbar^2}{2m}\nabla_{\mathbf{r}_2}^2 + V(r_1) + V(r_2) + \frac{e^2}{|\mathbf{r}_2 - \mathbf{r}_1|},$$
$$(1)$$

where $V(r) = -(V_0/r_0^2)\exp(-r/r_0)$, $\mathbf{r}_i$ the position operator of electron $i = 1,2$, and r_0 and V_0 determine the range and depth of the dot potential, respectively. After rescaling with r_0, in atomic units the Hamiltonian of Eq. (1) can be written as

$$H = -\frac{1}{2}\nabla_{\mathbf{r}_1}^2 - \frac{1}{2}\nabla_{\mathbf{r}_2}^2 - V_0 e^{-r_1} - V_0 e^{-r_2} + \frac{\lambda}{|\mathbf{r}_2 - \mathbf{r}_1|}, \quad (2)$$

where $\lambda = r_0$.

We choose the exponential binding potential to take advantage of its analytical properties. In particular, this potential is well-behaved and the energy of the resonance states can be calculated using complex scaling methods. So, besides its simplicity, the exponential potential allows us to independently obtain the energy of the resonance state and to check our results. The threshold energy ε of the Hamiltonian Eq. (2) (i.e., the one-body ground state energy) can be calculated exactly [24] and is given by

$$J_{2\sqrt{2\varepsilon}}(\sqrt{2V_0}) = 0, \quad (3)$$

where $J_\nu(x)$ is the Bessel function.

The discrete spectrum and the resonance states of the model given by Eq. (2) can be obtained approximately using $\mathcal{L}^2$ variational functions [17,25]. So, if $|\psi_j(1,2)\rangle$ are the exact eigenfunctions of the Hamiltonian, we look for variational approximations

$$|\psi_j(1,2)\rangle \simeq |\Psi_j(1,2)\rangle = \sum_{i=1}^{M} c_i^{(j)}|\Phi_i\rangle,$$
$$c_i^{(j)} = [\mathbf{c}^{(j)}]_i; \quad j = 1,\ldots,M, \quad (4)$$

where the $|\Phi_i\rangle$ must be chosen adequately and M is the basis-set size.

Since we are interested in the behavior of the system near the ground-state ionization threshold, we choose as basis set s-wave singlets given by

$$|\Phi_i\rangle \equiv |n_1,n_2;l\rangle = [\phi_{n_1}(r_1)\phi_{n_2}(r_2)]_s \mathcal{Y}_{0,0}^l(\Omega_1,\Omega_2)\chi_s, \quad (5)$$

where $n_2 \leqslant n_1$, $l \leqslant n_2$, χ_s is the singlet spinor, and the $\mathcal{Y}_{0,0}^l(\Omega_1,\Omega_2)$ are given by

$$\mathcal{Y}_{0,0}^l(\Omega_1,\Omega_2) = \frac{(-1)^l}{\sqrt{2l+1}} \sum_{m=-l}^{l} (-1)^m Y_{lm}(\Omega_1)Y_{l-m}(\Omega_2), \quad (6)$$

that is, they are eigenfunctions of the total angular momentum with zero eigenvalue and the Y_{lm} are the spherical harmonics. Note also that $\mathcal{Y}_{0,0}^l$ is a real function since it is symmetric in the particle index. The radial term $[\phi_{n_1}(r_1)\phi_{n_2}(r_2)]_s$ has the appropriate symmetry for a singlet state,

$$[\phi_{n_1}(r_1)\phi_{n_2}(r_2)]_s = \frac{\phi_{n_1}(r_1)\phi_{n_2}(r_2) + \phi_{n_1}(r_2)\phi_{n_2}(r_1)}{[2(1 + \langle n_1|n_2\rangle^2)]^{1/2}}, \quad (7)$$

where

$$\langle n_1|n_2\rangle = \int_0^\infty r^2 \phi_{n_1}(r)\phi_{n_2}(r)dr, \quad (8)$$

and the ϕ functions are chosen to satisfy $\langle n_1|n_1\rangle = 1$. The numerical results are obtained by taking the Slater-type forms for the orbitals:

$$\phi_n^{(\alpha)}(r) = \left[\frac{\alpha^{2n+3}}{(2n+2)!}\right]^{1/2} r^n e^{-\alpha r/2}, \quad (9)$$

where α is a nonlinear parameter of the basis. It is clear that, in terms of the functions defined in Eq. (5), the variational eigenfunctions reads as

$$\left|\Psi_i^{(\alpha)}(1,2)\right\rangle = \sum_{n_1 n_2 l} c_{n_1 n_2 l}^{(i),(\alpha)}|n_1,n_2;l;\alpha\rangle, \quad (10)$$

where $n_1 \geqslant n_2 \geqslant l \geqslant 0$, then the basis-set size is given by

$$M = \sum_{n_1=0}^{N}\sum_{n_2=0}^{n_1}\sum_{l=0}^{n_2} 1 = \frac{1}{6}(N+1)(N+2)(N+3), \quad (11)$$

so we refer to the basis-set size using both N and M. In Eq. (10), we added α as a basis index to indicate that, in general, the variational eigenfunction is α dependent. The matrix elements of the kinetic energy, the Coulomb repulsion between electrons, and other mathematical details involving the functions $|n_1,n_2;l;\alpha\rangle$ are given in Refs [26,27]. We only show here for completeness the matrix elements of the exponential potential in the basis of Eq. (9):

$$\langle n|e^{-r}|n'\rangle = \int_0^\infty \phi_n(r)\phi_{n'}(r)e^{-r}r^2 dr$$
$$= \left(\frac{\alpha}{1+\alpha}\right)^{n+n'+3} \frac{(2+n+n')!}{\sqrt{(2n+2)!(2n'+2)!}}. \quad (12)$$

Resonance states have isolated complex eigenvalues, $E_{\text{res}} = E_r - i\Gamma/2$, $\Gamma > 0$, whose eigenfunctions are not square-integrable. These states are considered as quasibound states
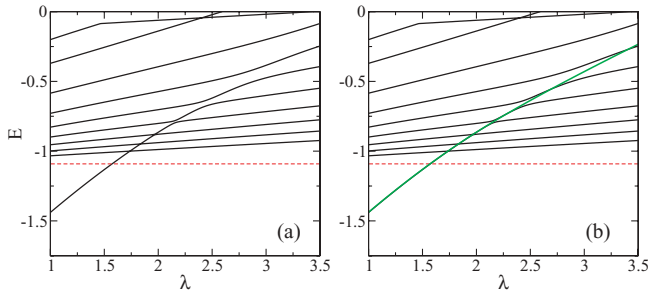
FIG. 1. (Color online) (a) Behavior of the variational eigenvalues $E_j^{(\alpha)}(\lambda)$ (black lines) for $N = 14$ and nonlinear parameter $\alpha = 2$. The red-dashed line corresponds to the threshold energy $\varepsilon \simeq -1.091$. Note that the avoided crossings between the variational eigenvalues are fairly visible. (b) The same variational eigenvalues as in (a) (black lines) and the energy calculated using the complex scaling method (green line) for a parameter $\theta = \pi/10$.

of energy E_r and inverse life time Γ. For the Hamiltonian Eq. (2), the resonance energies belong to the interval $(\varepsilon, 0)$ [16].

The resonance states can be analyzed using the spectrum obtained with a basis of $\mathcal{L}^2$ functions (see [19] and references therein). The levels above the threshold have several avoided crossings that "surround" the real part of the energy of the resonance state. The presence of a resonance can be made evident by looking at the eigenvalues obtained numerically. Figure 1 shows a typical spectrum obtained from the variational method. This figure shows the behavior of the variational eigenvalues $E_j^{(\alpha)}$ as functions of the parameter λ. The results shown were obtained using $N = 14$ and $\alpha = 2.0$. The value of α was chosen in order to obtain the best approximation for the energy of the ground state in the region of λ where it exists. The figure shows clearly that for $\lambda < \lambda_{\text{th}} \simeq 1.54$ there is only one bound state. Above the threshold, the variational approximation provides a finite number of solutions with energies below zero. Above the threshold ,there is not a clear-cut criterium to choose the value of the variational parameter. However, it is possible to calculate $E_r(\lambda)$ by calculating $E_j^{(\alpha)}$ for many different values of the variational parameter (see Kar and Ho [28]).

Figures 2(a) and (b) shows the numerical results for the first and second eigenvalues, respectively, for different values
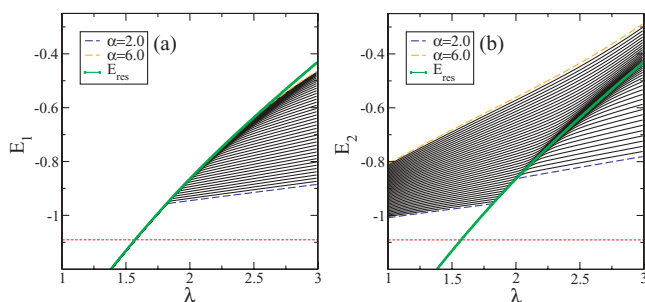

FIG. 2. (Color online) (a) First variational state energy versus λ for different values of the variational parameter α. From bottom to top α increases from $\alpha = 2$ (blue-dashed line) to $\alpha = 6$ (orange-dashed line). The real part of the resonance eigenvalue obtained using complex scaling ($\theta = \pi/10$) is also shown (green line). (b) Same as (a), but for the second-state energy.

of the variational parameter α. The figure also shows the behavior of the ground state (below the threshold) and the real part of the energy of the resonance calculated using complex scaling (above the threshold); this curve is used as a reference. The behavior of the smaller variational eigenvalue $E_1^{(\alpha)}(\lambda)$ is rather clear. Below the threshold, $E_1^{(\alpha)}(\lambda)$ is rather insensitive to the actual value of α; the differences between $E_1^{(\alpha=2)}(\lambda)$ and $E_1^{(\alpha=6)}(\lambda)$ are smaller than the width of the lines shown in the figure. Above the threshold, the behavior changes, and the curve for a given value of α has two well-defined regions; in each region E_1 is basically a straight line. The two straight lines in each region have different slopes and the change in the slope is located around $E_r(\lambda)$.

In the case of $E_2^{(\alpha)}(\lambda)$, there are three regions, and in each of them the curve for a given value of α is basically a straight line, and the slope is different in each region. A feature that appears rather clearly is that, for fixed λ, the density of levels for energy unit is not uniform, despite the curves $E_j^{(\alpha_i)}(\lambda)$ being drawn for forty equally spaced α_i between $\alpha = 2.0$ and $\alpha = 6.0$. This fact has been observed previously [29] and the density of states can be written in terms of two contributions: a localized one and an extended one. The localized density of states is attributed to the presence of the resonance state and, conversely, the extended density of states is attributed to the continuum of states between $(\varepsilon, 0)$.

The localized density of states $\rho(E)$ can be expressed as [28,29]

$$\rho(E) = \left| \frac{\partial E(\alpha)}{\partial \alpha} \right|^{-1}. \tag{13}$$

Since we are dealing with a variational approximation, we calculate

$$\rho\left[E_j^{(\alpha_i)}(\lambda)\right] = \left| \frac{E_j^{(\alpha_{i+1})}(\lambda) - E_j^{(\alpha_{i-1})}(\lambda)}{\alpha_{i+1} - \alpha_{i-1}} \right|^{-1}. \tag{14}$$

Figure 3 shows the typical behavior of $\rho_j(E) \equiv \rho[E_j^{(\alpha_i)}(\lambda)]$ for several eigenenergies and $\lambda = 2.25$. The real and imaginary parts of the resonance's energy, $E_r(\lambda)$ and Γ, respectively, can be obtained from $\rho(E)$ (see, for example, [28] and references therein). This method provides and independent way to obtain E_{res}, besides the method of complex scaling.

The values of $E_r(\lambda)$ and $\Gamma(\lambda)$ are obtained by performing a nonlinear fitting of $\rho(E)$ with the Lorentzian function

$$\rho(E) = \rho_0 + \frac{A}{\pi} \frac{\Gamma/2}{[(E - E_r)^2 + (\Gamma/2)^2]}. \tag{15}$$

One of the drawbacks of this method is evident: for each λ there are several $\rho_j(E)$ (in fact one for each variational level), and since each $\rho_j(E)$ provides a value for $E_r^j(\lambda)$ and $\Gamma^j(\lambda)$, one has to choose which one is the best. Kar and Ho [28] solve this problem by fitting all the $\rho_j(E)$ and keeping as the best values for $E_r(\lambda)$ and $\Gamma(\lambda)$ the fitting parameters with the smaller χ^2 value. At least for their data the best fitting (the smaller χ^2) usually corresponds to the larger n. This fact has the clear interpretation that if the numerical method approximates $E_r(\lambda)$ with $E_n^{(\alpha)}(\lambda)$, a large n means that the numerical method is able to provide a large number of approximate levels, and so the continuum of states between $(\varepsilon, 0)$ is "better" approximated.
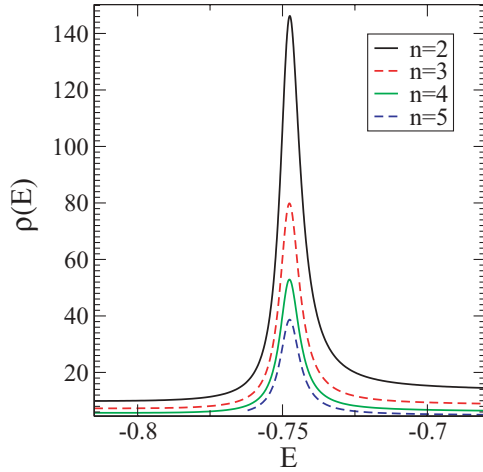
FIG. 3. (Color online) Density of states $\rho(E)$ for $\lambda = 2.25$ and basis-set size $N = 14$. The results were obtained using Eq. (13) and correspond to, from top to bottom, the second (black line), third (red-dashed line), fourth (green line), and fifth (blue-dashed line) levels.

It is worth remarking that the results obtained from the complex scaling method and from the density of states are in excellent agreement (see Table I).

III. FIDELITY AND DOUBLE-ORTHOGONALITY FUNCTIONS

Since the work of Zanardi *et al.* [20,21], there has been a growing interest in the fidelity approach as a means to study quantum phase transitions [20], the information-theoretic differential geometry on quantum phase transitions (QPTs) [21], or the disordered quantum XY model [22]. In all these cases, the fidelity is used to detect the change of behavior of the states of a quantum system. For example, if λ is the external parameter that drives a system through a QPT, the fidelity is the superposition $\mathcal{F} = \langle \Psi(\lambda - \delta\lambda), \Psi(\lambda + \delta\lambda) \rangle$, where Ψ is the ground state of the system. It has been shown that $\mathcal{F}$ is a good detector of critical behavior in ordered [20] and disordered systems [22].

In the following, we will show that the energy levels calculated using the variational approximation show critical

behavior near the energy of the resonance and, moreover, that the curve $E_r(\lambda)$ can be obtained from the fidelity.

Figure 4 shows the behavior of the function $\mathcal{G}_n = 1 - F_n$, where $F_n = |\langle \Psi_n(\lambda), \Psi_n(\lambda + \delta\lambda) \rangle|^2$, and Ψ_n is the nth eigenstate obtained with the variational approach.

The behavior of $\mathcal{G}$ is quite simple. The value of $\mathcal{G}$ is very small, except near the avoided crossings where the value of $\mathcal{G}$ increases rather steeply (at least for small n). This is so because near the avoided crossing the superposition $|\langle \Psi_n(\lambda), \Psi_n(\lambda + \delta\lambda) \rangle|^2 \to 0$. Actually, $|\langle \Psi_n(\lambda), \Psi_n(\lambda + \delta\lambda) \rangle|^2 \to 0$ near points such that $E_n^{(\alpha)}(\lambda)$ has nonanalytical behavior. Is for this reason that the fidelity is a good detector of quantum phase transitions [20–22]. In a first-order QPT the energy of the ground state is nonanalytical, and in a second-order QPT the gap in the avoided crossing between the ground state and the first excited state goes to zero in the thermodynamic limit.

The previous argument supports why $\mathcal{G}_1$ has only one peak, while all the others functions $\mathcal{G}_n$ have two peaks, where the number of peaks is the number of avoided crossings of each level. However, since the resonance state lies somewhere between the avoided crossings it is natural to ask what feature of the fidelity signals the presence of the resonance. For a given level n, the value of the energy is fixed, so we must pick a distinctive feature of $\mathcal{G}_n$ that is present for some λ_n^f such that $E_r(\lambda_n^f) \simeq E_n(\lambda_n^f)$ (from hereon we will use E_n or $E_n^{(\alpha)}$ interchangeably). The result is that λ_n^f is the value of λ such that $\mathcal{G}_n$ attains its minimum between its two peaks. Figure 4 shows the points $E_n(\lambda_n^f)$. In Table I we tabulate the real part of the energy calculated using DO, complex scaling, fidelity, and density of states for the five values of λ_n^f shown in Figure 4. The numerical values obtained using the fidelity and density-of-states methods are identical up to five figures. The relative error between the energies obtained is less than 0.25%.

The idea of detecting the resonance state energy with functions depending on the inner product could be taken a step further. To this end we consider the DO functions

$$\mathcal{D}_n(\lambda) = |\langle \Psi_n(\lambda_L), \Psi_n(\lambda) \rangle|^2 + |\langle \Psi_n(\lambda_R), \Psi_n(\lambda) \rangle|^2,$$
$$\text{for} \quad \lambda_L < \lambda < \lambda_R, \tag{16}$$

where λ_L and λ_R are two given coupling values. It is clear from the definition that $0 \leqslant \mathcal{D}_n(\lambda) \leqslant 2$. If there are not

TABLE I. Resonance Energy obtained by four different methods. Basis size is $N = 14$.

| $\lambda_{\mathcal{D}}^n$		$\mathcal{D}_n$	Complex Scaling	Fidelity and density of states				
				$n = 2$	$n = 3$	$n = 4$	$n = 5$	$n = 6$
1.755 $(n = 2)$	E	−0.99075	−0.99098	−0.99011				
	α	2.0	2.0	1.560				
1.8625 $(n = 3)$	E	−0.93427	−0.93452	−0.93434	−0.93383	−0.93303		
	α	2.0	2.0	2.448	1.787	1.414		
2.02 $(n = 4)$	E	−0.85498	−0.85556	−0.85581	−0.85564	−0.85531	−0.85486	
	α	2.0	2.0	3.339	2.435	1.906	1.519	
2.255 $(n = 5)$	E	−0.74329	−0.74538	−0.74518	−0.74527	−0.74519	−0.74521	−0.74514
	α	2.0	2.0	4.262	3.098	2.414	1.936	1.574
2.61 $(n = 6)$	E	−0.58276	−0.59077	−0.58825	−0.58910	−0.58942	−0.58965	−0.58979
	α	2.0	2.0	5.248	3.799	3.799	2.373	1.936
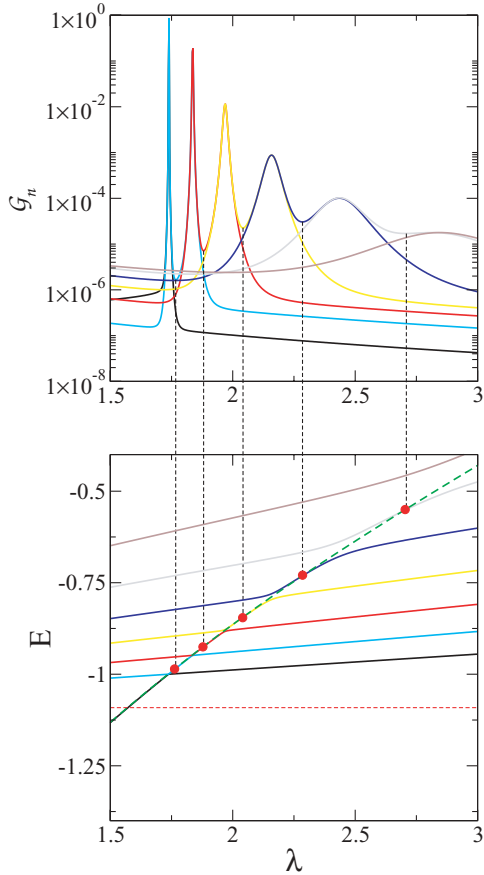
FIG. 4. (Color online) The upper panel shows the behavior of $\mathcal{G}_n$, for $n = 1, \ldots, 7$. Each function $\mathcal{G}_n$ has two peaks, except for $n = 1$. Since one of the peaks of $\mathcal{G}_n$ coincides with one of the peaks of $\mathcal{G}_{n+1}$, only one peak for each level n is apparent. From left to right the visible line at each peak corresponds to $n = 2, \ldots, 7$ (cyan, red, yellow, blue, grey, and brown lines, respectively). The $n = 1$ line has no visible peak (black). The lower panel shows the variational eigenlevels $n = 1, \ldots, 7$ (with the same color convention used as in the upper panel), and $E_r(\lambda)$ (green-dashed line). The black vertical dashed lines connecting both panels show the value of λ where each $\mathcal{G}_n$ has its minimum, λ_n^f. The red dots in the lower panel correspond to $E_n(\lambda_n^f)$.

resonances between λ_L and λ_R, the wave function is roughly independent of λ so $\mathcal{D}_n(\lambda) \simeq 2$. However, the scenario is different when a resonance is present between λ_L and λ_R. In this case, the avoided crossings for a given state Ψ_n are located approximately at λ_L^{av} and λ_R^{av}, where $L(R)$ stands for the leftmost (rightmost) avoided crossing. Requesting that $\lambda_L < \lambda_L^{av} < \lambda_R^{av} < \lambda_R$, it follows that $\langle \Psi_n(\lambda_L) | \Psi_n(\lambda_R) \rangle \simeq 0$. With this prescription, the $\mathcal{D}_n$ functions are rather independent of the actual values chosen for λ_L and λ_R. For a given n, $\mathcal{D}_n(\lambda)$ measures how much the state $\Psi_n(\lambda)$ differs from the extended states $\Psi_n(\lambda_R)$ and $\Psi_n(\lambda_L)$.

We look for the states with minimum $\mathcal{D}_n$ in the same fashion as we did with the fidelity, and we can obtain values $E_r(\lambda_{\mathcal{D}}^n) \simeq E_n(\lambda_{\mathcal{D}}^n)$, where $\lambda_{\mathcal{D}}^n$ is defined by $\mathcal{D}_n(\lambda_{\mathcal{D}}^n) = \min_\lambda \mathcal{D}_n(\lambda)$. Figure 5 shows the behavior of $\mathcal{D}_n$ obtained for the same parameters that the ones used in Figure 4, and we compare the values of $E_n(\lambda_{\mathcal{D}}^n)$ with energy values obtained using complex
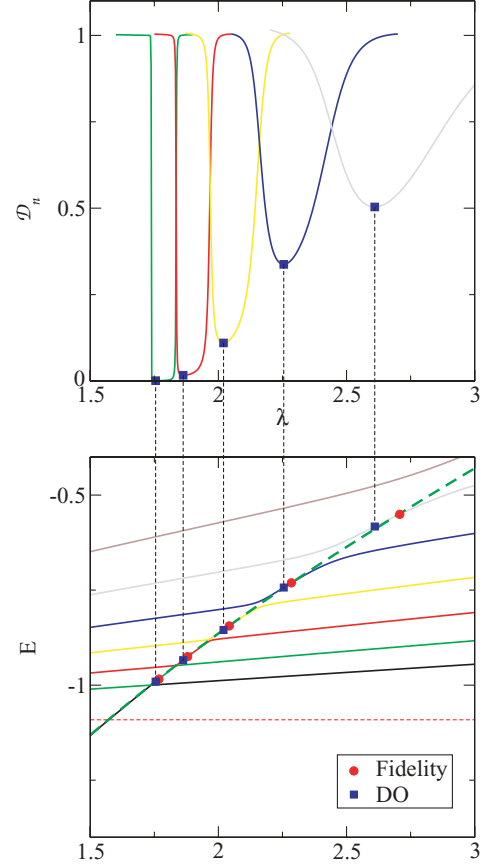

FIG. 5. (Color online) The lower panel shows the variational energy levels $E_n(\lambda)$, from bottom to top, for $n = 1, \ldots, 7$ (the black, green, red, yellow, blue, grey, and brown continuous lines, respectively); $E_r(\lambda)$ (the dark-green-dashed line); $E_n(\lambda_{DO}^n)$ (blue squares); and $E_n(\lambda_n^f)$ (red dots). The upper panel shows the behavior of $\mathcal{D}_n$ versus λ for $n = 2, \ldots, 7$. The color convention for the $\mathcal{D}_n$ is the same as used in the lower panel. The black-dot-dashed vertical lines show the location of the points $\lambda_{\mathcal{D}}^n$.

scaling methods in Table I. The curves in Figure 5 show that outside (λ_L, λ_R), the states Ψ_n change very little when λ changes and $\mathcal{D}_n \simeq 1$. Inside the resonance region $(\lambda_L^{av}, \lambda_R^{av})$, the functions $\mathcal{D}_n$ change abruptly. The width in λ in which a given $\mathcal{D}_n$ changes abruptly apparently depends on the width Γ of the resonance, but so far we have not been able to relate both quantities.

From Table I and Figure 5, it is rather clear that despite the fidelity and the $\mathcal{D}_n$ providing approximate values for $E_r(\lambda)$ for different sets of λ, both sets belongs to the "same" curve (i.e., the same curve considering the numerical inaccuracies). Both methods would give the same results when $|\lambda_R^{av} - \lambda_L^{av}| \to 0$, but for finite N the fidelity measures how fast the state changes when $\lambda \to \lambda + \Delta\lambda$ and the $\mathcal{D}_n$ measures how much a state differs from the extended states located at both sides of the resonance state.

IV. THE ENTROPY

If $\hat{\rho}^{\text{red}}$ is the reduced-density operator for one electron [19], then the von Neumann entropy $\mathcal{S}$ is given by

$$\mathcal{S} = -\text{tr}(\hat{\rho}^{\text{red}} \log_2 \hat{\rho}^{\text{red}}), \tag{17}$$

and the linear entropy S_{lin} is given by [11]

$$\mathcal{S}_{lin} = 1 - \text{Tr}[(\hat{\rho}^{red})^2], \qquad (18)$$

where the reduced-density operator is

$$\hat{\rho}^{red}(\mathbf{r}_1, \mathbf{r}_1') = \text{Tr}_2 |\Psi\rangle\langle\Psi|, \qquad (19)$$

where the trace is taken over one electron and $|\Psi\rangle$ is the total two-electron wave function. Both entropies, Eqs. (17) and (18), can be used to analyze how much entanglement a given state has. One can choose between one entropy or the other out of convenience. In this article, we will use the linear entropy. For a discussion about the similarities between the two entropies see Ref. [11] and references therein.

As the two-electron wave function is not available, we instead use the variational approximation Eq. (10). As has been noted in previous works (see [5] and references therein), when the total wave function factorizes in spatial and spinorial components it is possible to single out both contributions, so the analysis of the behavior of the entropy is reduced to the analysis of the behavior of the spatial part S, since the spinorial contribution is constant. In this case, if $\varphi(\mathbf{r}_1, \mathbf{r}_2)$ is the two-electron wave function and $\rho^{red}(\mathbf{r}_1, \mathbf{r}_1')$ is given by

$$\rho^{red}(\mathbf{r}_1, \mathbf{r}_1') = \int \varphi^{\star}(\mathbf{r}_1, \mathbf{r}_2)\varphi(\mathbf{r}_1', \mathbf{r}_2)\, d\mathbf{r}_2, \qquad (20)$$

then the linear entropy S_{lin} can be calculated as

$$S_{lin} = 1 - \sum_i \lambda_i^2, \qquad (21)$$

where the λ_i are the eigenvalues of ρ^{red} and are given by

$$\int \rho^{red}(\mathbf{r}_1, \mathbf{r}_1')\phi_i(\mathbf{r}_1')d\mathbf{r}_1' = \lambda_i \phi_i(\mathbf{r}_1). \qquad (22)$$

Figure 6 shows the behavior of the linear entropy for several variational levels. The meaning of each curve has been extensively discussed in Ref. [19]. We include a brief discussion here for completeness.

When the two-electron quantum dot loses an electron, the state of the system can be described as one electron bound
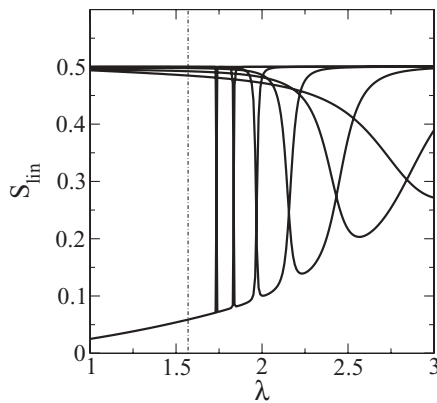
to the dot potential, and one unbound electron at infinity. As a consequence, the spatial wave function can be written as a symmetrized product of one-electron wave functions, so $S_{lin} = S_c = 1/2$. Therefore, if only bound and continuum states are considered, the entropy has a discontinuity when λ crosses the threshold value λ_{th}. The picture changes significantly when resonance states are considered. The resonance state keeps its two electrons "bound" before the ionization for a finite time given by the inverse of the imaginary part of the energy. Of course, the life time of a bound state is infinite while the life time of a resonance state is finite. Reference [19] suggests that it is possible to construct a smooth function $S[E_r(\lambda)]$ that "interpolates" between the minima of the functions $S(\Psi_j)$ shown in Figure 6. This assumption was justified by arguments similar to those used in the present work; that is, if we call λ_n^S the value of λ where $S(\Psi_n)$ is minimum, then $E_n(\lambda_n^S)$ follows approximately the curve $E_r(\lambda)$. As Ferrón *et al.* [19] used only one variational parameter α, it seemed natural to pick the minimum value of $S(\Psi_n)$ as the feature that signaled the presence of the resonance state.

Until now we have exploited the fact that $E_r(\lambda)$ at a given λ can be approximated by variational eigenvalues corresponding to different values of the variational parameter, say $E_r(\lambda) \simeq E_n^{(\alpha)}(\lambda) \simeq E_{n'}^{(\alpha')}(\lambda)$ (the superscript α is made evident to remark that the eigenvalues correspond to different variational parameters α and α'). There is no problem in approximating an exact eigenvalue with different variational eigenvalues. But, from the point of view of the entropy, there is a problem since, in general, $S[\Psi_n^{(\alpha)}(\lambda)]$ is not close to $S[\Psi_n^{(\alpha')}(\lambda)]$. Moreover, as has been stressed in Ref. [2], a given numerical method could be useful to accurately calculate the spectrum of a quantum system, but hopelessly inaccurate to calculate the entanglement. In few-body systems there is evidence that there is a strong correlation between the entanglement and the Coulomb repulsion between the components of the system [5,9,11,26]. Because of this correlation, we will carefully investigate the behavior of the Coulomb repulsion between the electrons in our model.

For the Hamiltonian Eq. (2), and for $\psi \in \mathcal{L}^2$ being an eigenvector of H with eigenvalue E, the Hellman-Feynman theorem states that

$$\frac{\partial E}{\partial \lambda} = \langle\psi| \frac{1}{r_{12}} |\psi\rangle. \qquad (23)$$

We use both sides of Eq. (23) to analyze how the variational approximation works with expectation values of observables that are not the Hamiltonian. The right-hand side of Eq. (23) is well defined if we use $\mathcal{L}^2$ functions as the approximate variational eigenfunctions.

To evaluate the left-hand side of Eq. (23), we take advantage that we have found, independently, the real part of the resonance eigenvalue, $E_r(\lambda)$, using complex scaling methods. Figure 7 shows the behavior of $dE_r/d\lambda$ and the Coulomb repulsion between the two electrons, $\langle 1/r_{12}\rangle_n$, where $\langle\cdots\rangle_n$ stands for the expectation value calculated with $\Psi_n^{(\alpha)}$. The behavior of $\langle 1/r_{12}\rangle_n$ is quite simple to analyze: where the linear entropy of $\Psi_n^{(\alpha)}$ has a valley the expectation value $\langle 1/r_{12}\rangle_n$ has a peak. Where the expectation value $\langle 1/r_{12}\rangle_n$ has its maximum the corresponding linear entropy has its minimum. The inverse
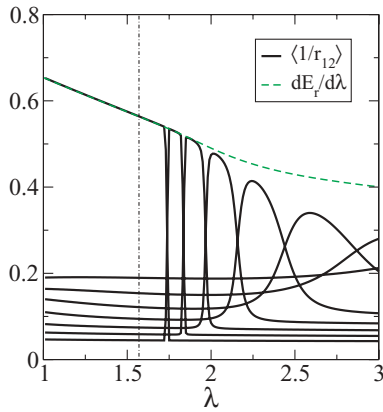

FIG. 6. Behavior of $S_{lin}[\Psi_j^{(\alpha)}]$, where the $\Psi_j^{(\alpha)}$ are the variational eigenstates corresponding to the first seven energy levels shown in Fig. 1 for $N = 14$ and $\alpha = 2.0$. All the curves $S_{lin}[\Psi_j^{(\alpha)}]$, except for the corresponding to $S_{lin}[\Psi_1^{(\alpha)}]$, have a single minimum located at λ_j^S; that is, $S_{lin}[\Psi_j^{(\alpha)}(\lambda_j^S)] = \min_\lambda S_{lin}[\Psi_j^{(\alpha)}(\lambda)]$. If $i < j$, then $\lambda_i^S < \lambda_j^S$.

FIG. 7. Expectation values of the Coulomb repulsion for the variational states $\Psi_n^{(\alpha)}$, $n = 1, \ldots, 8$ with $N = 14$ and $\alpha = 2.0$. Also shown is the curve $\partial E_r / \partial \lambda$ obtained from the complex energy of the complex scaling method.

behavior showed by the entropy and the Coulomb repulsion has been observed previously [11,26].

For a given variational parameter α and for small n, $\langle 1/r_{12} \rangle_n$ has its maximum very close to the curve $dE_r/d\lambda$. Besides, the shape of both curves near the maximum of $\langle 1/r_{12} \rangle_n$ is very similar, in this sense our variational approach gives a good approximation not only for $E_r(\lambda)$, but for its derivative too.

For larger values of n the maximum of $\langle 1/r_{12} \rangle_n$ deviates from the curve of $dE_r/d\lambda$, and the shape of the curves near this maximum is quite different. We proceed as before and changing α we obtain a good approximation for $dE_r/d\lambda$ up to a certain value λ_{rep}. For any λ smaller than λ_{rep}, there is a pair n,α such that $\langle 1/r_{12} \rangle_{n,\alpha}$ is locally close to $dE_r/d\lambda$ and the slope of both curves is (up to numerical errors) the same, see Fig. 8.

Apparently there is no way to push further the variational method, at least keeping the same basis set, in order to obtain a better approximation than the depicted in Fig. 8. The difficulty seems to be more deep than just a limitation of the variational
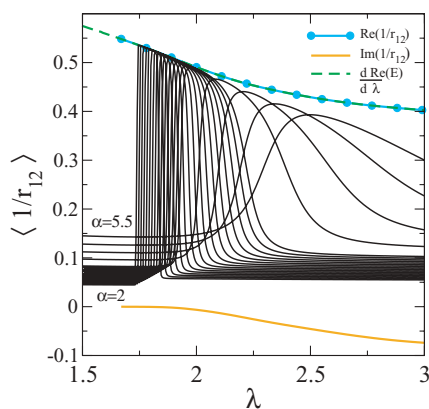
method used until this point. We can clarify this subject using the properties of the complex scaling method. Let us call ϕ^θ the eigenvector such that

$$H(\theta)\phi^\theta = E_{\text{res}}\phi^\theta, \tag{24}$$

where $H(\theta)$ is the Hamiltonian obtained from the complex scaling transformation [30], and θ is the angle of "rotation." The eigenvector ϕ^θ depends on θ, but for θ large enough the eigenvalue E_{res} does not depend on θ. As pointed by Moiseyev [30], the real part of the expectation value of a complex scaled observable is the physical measurable quantity, while the imaginary part gives the uncertainty of measuring the real part. Moreover, the physical measurable quantity must be θ-independent as is, for example, the eigenvalue E_{res}.

The eigenvector ϕ^θ can be normalized using

$$\langle (\phi^\theta)^\star | \phi^\theta \rangle = 1. \tag{25}$$

Since ϕ^θ is normalized, we get

$$\frac{\partial E_{\text{res}}}{\partial \lambda} = \langle (\phi^\theta)^\star | \frac{e^{-i\theta}}{r_{12}} | \phi^\theta \rangle = \left\langle \frac{1}{r_{12}} \right\rangle_\theta, \tag{26}$$

where we have used that, under the complex scaling transformation,

$$\frac{1}{r_{12}} \rightarrow \frac{e^{-i\theta}}{r_{12}}, \tag{27}$$

and we have defined the quantity $\langle \frac{1}{r_{12}} \rangle_\theta$. This generalized Hellman-Feynman theorem is also valid for Gamow states [31].

Figure 8 shows the behavior of the expectation value in the $\langle \frac{1}{r_{12}} \rangle_\theta$ as a function of λ. It is clear that the real part of the expectation value $\langle \frac{1}{r_{12}} \rangle_\theta$ coincides with $\partial E_r/\partial \lambda$. More interestingly, λ_{rep} is where the imaginary part of $\langle \frac{1}{r_{12}} \rangle_\theta$ became noticeable. From this fact, we conclude that it is not possible to adequately approximate the Coulomb repulsion of a resonance state or its entropy with only real $\mathcal{L}^2$-variational functions, despite its success when dealing with the resonance-state spectrum.

We define the complex scaled density operator of the resonance state by

$$\rho^\theta = |\phi^\theta\rangle\langle(\phi^\theta)^\star| \tag{28}$$

and the complex linear entropy by

$$S^\theta = 1 - \text{Tr}(\rho_{\text{red}}^\theta)^2, \tag{29}$$

where

$$\rho_{\text{red}}^\theta = \text{Tr}_2 \rho^\theta, \tag{30}$$

and ϕ^θ is the eigenvector of Eq. (24). This definition is motivated by the fact that the density operator should be the projector onto the space spanned by $|\phi^\theta\rangle$. Because the normalization Eq. (25) requires the bra to be conjugated, ρ^θ is the adequate projector to use.

Because of the normalization Eq. (25), we have that $\text{Tr}\rho^\theta = \text{Tr}\rho_{\text{red}}^\theta = 1$, despite both density operators having complex eigenvalues.

Figure 9 shows that up to a certain value of λ the real part of S^θ follows closely an envelope containing the minima of

FIG. 8. (Color online) Expectation value $\langle 1/r_{12} \rangle_2^{(\alpha)}$ versus λ for a basis size $N = 14$ and $\alpha = 2, \ldots, 3.5$ in steps of 0.1 and for $\alpha = 4, \ldots, 5.5$ in steps of 0.5 (black solid lines). The real (cyan dotted) and imaginary (orange line) parts of $\langle 1/r_{12} \rangle_\theta$ ($\theta = \pi/10$) and the derivative of the real part of the complex-scaled energy are also shown.
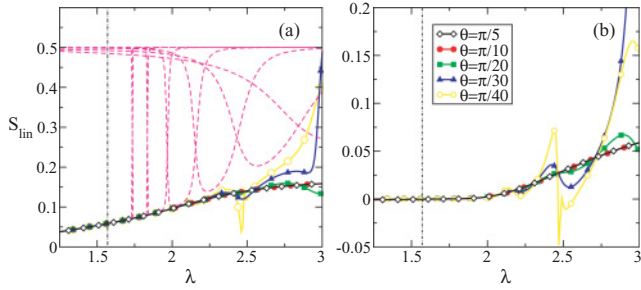
FIG. 9. (Color online) Panel (a) shows the linear entropy for the same values as in Fig. 6 (magenta-dashed lines). Also shown is the real part of the complex linear entropy for several values of the complex rotation angle $\theta = \frac{\pi}{5}, \frac{\pi}{10}, \frac{pi}{20}, \frac{\pi}{30}, \frac{\pi}{40}$ (black-empty diamonds, red dots, green squares, blue triangle, yellow-empty dots). Panel (b) shows the imaginary part of the complex linear entropy for the same values as in (a).

the functions $S(\Psi_n)$. However, for large enough λ, S^θ departs from the functions $S(\Psi_n)$. It is worth mentioning that for large enough θ, S^θ does not depend on θ. On the other hand, far away from the threshold, the complex scaling requires larger values of θ to isolate the resonance state eigenenergy, but in this regime the method becomes unstable. Because of the numerical evidence, near the threshold the entropy calculated by Ferrón *et al.* is basically correct, but for larger values of λ the amount of entanglement of the resonance state should be characterized by S^θ and not by any of the $S(\Psi_n)$.

V. SUMMARY AND CONCLUSIONS

We have presented numerical calculations about the behavior of the fidelity and the double-orthogonality functions $\mathcal{D}_n(\lambda)$. The numerical results show that, for selected values of λ, it is possible to obtain $E_r(\lambda)$ with great accuracy without employing any stabilization method. These two methods to find $E_r(\lambda)$ do not depend on any particular assumptions about the model or the variational method used to find approximate eigenfunctions above the threshold. Rather, their success depends on the ability of the approximate eigenstates to detect the nonanalytical changes in the spectrum.

The fidelity has been extensively used to detect quantum phase transitions in spin systems [20], to study the behavior of quasi-integrable systems [32], thermal phase transitions [33], etc. This work applies the concept of fidelity to resonance states and to the characterization of spectral properties of a system with non-normalizable eigenstates. Besides, it is remarkable that the fidelity and the double orthogonality give the real part of the resonance eigenvalue using only real variational functions. This energy as a function of λ is obtained by moving the nonlinear parameter α but without fitting, as is required by standard stabilization methods. Moreover, as shown by the tabulated values in Table I, the fidelity provides $E_r(\lambda)$ as accurately as the density-of-states method, with considerably less numerical effort.

We proposed a definition of the resonance entropy based on a complex scaled extension of the usual definition. The extension implies that the reduced density operator is not hermitian and has complex eigenvalues, resulting in a complex entropy. The real and imaginary parts of the complex entropy are θ-independent, as should be expected for the expectation value of an observable [30]. This independence supports the interpretation of the real part of the entropy as being the amount of entanglement of the resonance state.

Other kinds of resonances, such as those that arise from the perturbation of bound states embedded in the continuum, could be studied by applying the same quantum-information methods used in this article, and work is in progress in this direction.

[1] A. Osterloh, L. Amico, G. Falci, and R. Fazio, Nature (London) **416**, 608 (2002).

[2] Norbert Schuch, Michael M. Wolf, Frank Verstraete, and J. I. Cirac, Phys. Rev. Lett. **100**, 030504 (2008).

[3] W. K. Wootters, Phys. Rev. Lett. **80**, 2245 (1998).

[4] Longyan Gong and Peiqing Tong, Phys. Rev. B **78**, 115114 (2008); Wing-Chi Yu, Ho-Man Kwok, Junpeng Cao, and Shi-Jian Gu, Phys. Rev. E **80**, 021108 (2009); David Schwandt, Fabien Alet, and Sylvain Capponi, Phys. Rev. Lett. **103**, 170501 (2009).

[5] O. Osenda and P. Serra, Phys. Rev. A **75**, 042331 (2007).

[6] O. Osenda and P. Serra, J. Phys. B **41**, 065502 (2008).

[7] F. Schmüser and Dominik Janzing, Phys. Rev. A **73**, 052313 (2006).

[8] Yan Liu, Yujun Zheng, Weiyi Ren, and Shiliang Ding, Phys. Rev. A **78**, 032523 (2008).

[9] J. P. Coe, A. Sudbery, and I. D'Amico, Phys. Rev. B **77**, 205122 (2008).

[10] Clive Emary, Phys. Rev. B **80**, 161309(R) (2009); Robert Roloff and Walter Pötz, *ibid.* **76**, 075333 (2007).

[11] S. Abdullah, J. P. Coe, and I. D'Amico, Phys. Rev. B **80**, 235302 (2009).

[12] L. Sælen, R. Nepstad, I. Degani, and J. P. Hansen, Phys. Rev. Lett. **100**, 046805 (2008).

[13] Daniel Loss and David P. DiVincenzo, Phys. Rev. A **57**, 120 (1998).

[14] A. Imamoḡlu, D. D. Awschalom, G. Burkard, D. P. DiVincenzo, D. Loss, M. Sherwin, and A. Small, Phys. Rev. Lett. **83**, 4204 (1999).

[15] Y. Sajeev and N. Moiseyev, Phys. Rev. B **78**, 075316 (2008).

[16] W. P. Reinhardt and Seungsuk Han, Int. J. Quantum Chem. **57**, 327 (1996).

[17] M. Bylicki, W. Jaskólski, A. Stachów, and J. Diaz, Phys. Rev. B **72**, 075434 (2005).

[18] J. Dubau and I. A. Ivanov, J. Phys. B **31**, 3335 (1998).

[19] A. Ferrón, O. Osenda, and P. Serra, Phys. Rev. A **79**, 032509 (2009).

[20] P. Zanardi and N. Paunković, Phys. Rev. E **74**, 031123 (2006).

[21] P. Zanardi, P. Giorda, and M. Cozzini, Phys. Rev. Lett. **99**, 100603 (2007).

[22] S. Garnerone, N. T. Jacobson, S. Haas, and P. Zanardi, Phys. Rev. Lett. **102**, 057205 (2009).

[23] F. M. Pont and P. Serra, J. Phys. A **41**, 275303 (2008).

[24] A. Galindo and S. Pascual, *Quantum Mechanics* (Springer Verlag, Berlin, 1990).

[25] A. T. Kruppa and K. Arai, Phys. Rev. A **59**, 3556 (1999).

[26] O. Osenda, P. Serra, and S. Kais, Int. J. Quantum. Inform. **6**, 303 (2008).

[27] P. Serra and S. Kais, Chem. Phys. Lett. **372**, 205 (2003).

[28] Sabyasachi Kar and Y. K. Ho, J. Phys. B **37**, 3177 (2004).

[29] V. A. Mandelshtam, T. R. Ravuri, and H. S. Taylor, Phys. Rev. Lett. **70**, 1932 (1993).

[30] N. Moiseyev, Phys. Rep. **302**, 212 (1998).

[31] P. Ziesche, K. Kunze, and B. Milek, J. Phys. A **20**, 2859 (1987).

[32] Yaakov S. Weinstein, and C. S. Hellberg, Phys. Rev. E **71**, 016209 (2005).

[33] H. T. Quan and F. M. Cucchietti, Phys. Rev. E **79**, 031101 (2009).